Status of the KMOS multi-object near-infrared integral field spectrograph

Ray Sharples[*a], Ralf Bender[b,d], Alex Agudo Berbel[d], Richard Bennett[c], Naidu Bezawada[c], Michele Cirasuolo[c], Paul Clark[a], George Davidson[c], Richard Davies[d], Roger Davies[e], Marc Dubbeldam[a], Alasdair Fairley[c], Gert Finger[f], Reinhard Genzel[d], Reinhold Haefner[b], Achim Hess[b], Ian Lewis[e], David Montgomery[c], John Murray[c], Bernard Muschielok[b], Natascha Förster Schreiber[d], Jeff Pirard[f], Suzanne Ramsey[f], Phil Rees[c], Josef Richter[b], David Robertson[a], Ian Robson[c], Stephen Rolt[a], Roberto Saglia[b], Joerg Schlichter[b], Matthias Tecza[e], Stephen Todd[c], Michael Wegner[b], Erich Wiezorrek[d]

[a]Department of Physics, University of Durham, Durham, UK
[b]Universitätssternwarte München, München, Germany
[c]UK Astronomy Technology Centre, Royal Observatory, Edinburgh, UK
[d]Max-Planck-Institut für Extraterrestrische Physik, Garching, Germany
[e]Sub-Department of Astrophysics, University of Oxford, Oxford, UK
[f]European Southern Observatory, Garching, Germany

ABSTRACT

KMOS is a multi-object near-infrared integral field spectrograph being built by a consortium of UK and German institutes. We report on the final integration and test phases of KMOS, and its performance verification, prior to commissioning on the ESO VLT later this year.

Keywords: infrared spectrographs, integral field spectroscopy, multi-object spectroscopy

1. INTRODUCTION

KMOS is a unique cryogenic near-infrared (0.8 to 2.5 μm) multi-object spectrograph that uses deployable integral field units (d-IFUs) to obtain spatially-resolved spectra for multiple target objects selected from within an extended field of view[1]. KMOS will be mounted onto the Nasmyth B platform of VLT/UT1 (Antu) and will use the telescope A&G facilities. The top-level scientific requirements are: (i) to support spatially-resolved (3-D) spectroscopy; (ii) to allow multiplexed spectroscopic observations; (iii) to allow observations across any of the IZ, YJ, H, and K infrared atmospheric windows. These requirements have been flowed down[2] to the final system design specifications shown in Table 1. KMOS has just completed its final integration and test phases prior to shipment to the ESO Paranal Observatory in Chile. The as-built design employs 24 robotic arms that position fold mirrors at user-specified locations within a 7.2 arcmin diameter field-of-view[3]. Each arm selects a sub-field on the sky of 2.8x2.8 arcseconds. The size of the sub-fields is tailored specifically to match the compact sizes of high redshift galaxies, with a spatial sampling of 0.2 arcsec per pixel designed to sample the excellent infrared seeing at Paranal (<FWHM>=0.5 arcsec in the K-band). The sub-fields are then fed to 24 advanced image slicer IFUs that partition each sub-field into 14 slices with 14 spatial pixels along each slice[4]. Light from the IFUs is dispersed by three cryogenic grating spectrometers[5] which generate 14x14 spectra with ~1000 Nyquist-sampled spectral resolution elements for all of the 24 independent sub-fields. The spectrometers each employ a single 2kx2k Hawaii-2RG HgCdTe detector. The optical layout for the whole system has a threefold symmetry about the Nasmyth optical axis which has allowed a staged/modular approach to assembly, integration and test. The following sections present a detailed technical overview of the instrument and the as-built performance.

[*] r.m.sharples@durham.ac.uk; phone 44-191-334-3719; 44-191-334-3609; www.dur.ac.uk/cfai

Ground-based and Airborne Instrumentation for Astronomy IV, edited by Ian S. McLean, Suzanne K. Ramsay, Hideki Takami, Proc. of SPIE Vol. 8446, 84460K · © 2012 SPIE · CCC code: 0277-786X/12/$18 · doi: 10.1117/12.926021

Table 1: Final design specifications for the KMOS spectrograph.

Parameter	Final Design
Wavelength coverage	0.8 to 2.5 μm
Spectral Bands	IZ,YJ,H,K,H+K
Spectral Resolving Power	R=3400,3600,4000,4200,2000 (IZ,YJ,H,K,H+K)
Number of IFUs	24
Extent of each IFU	2.8 x 2.8 arcseconds
Spatial Sampling	0.2 x 0.2 arcseconds
Patrol field	7.2 arcmin diameter circle
Close packing of IFUs	≥ 3 within 1 sq. arcmin
Closest approach of IFUs	≥ 2 pairs of IFUs separated by 6 arcsec

2. TECHNICAL DESCRIPTION

2.1 Overview

From a hardware perspective the instrument partitions into the following key subsystems:

- Pickoff subsystem
- IFU subsystem
- Spectrograph subsystem
- Detector subsystem
- Infrastructure subsystems and electronics

The opto-mechanical parts of the instrument are all contained within a cryostat, operated at a temperature of 120K, whilst the electronics are on the Nasmyth platform and inside the cable rotator (CACOR; see Fig. 1)

KMOS has been designed to have effectively three independent modules, each of them comprising 8 pickoff arm systems, a set of 8 IFUs, one spectrograph and one 2kx2k HgCdTe near-IR detector. This ensures that in case of failure of one system, 2/3 of the functionality will still remain. The following sections describe the different sub-systems of KMOS in the order they are encountered along the optical path going from the telescope to the detector.

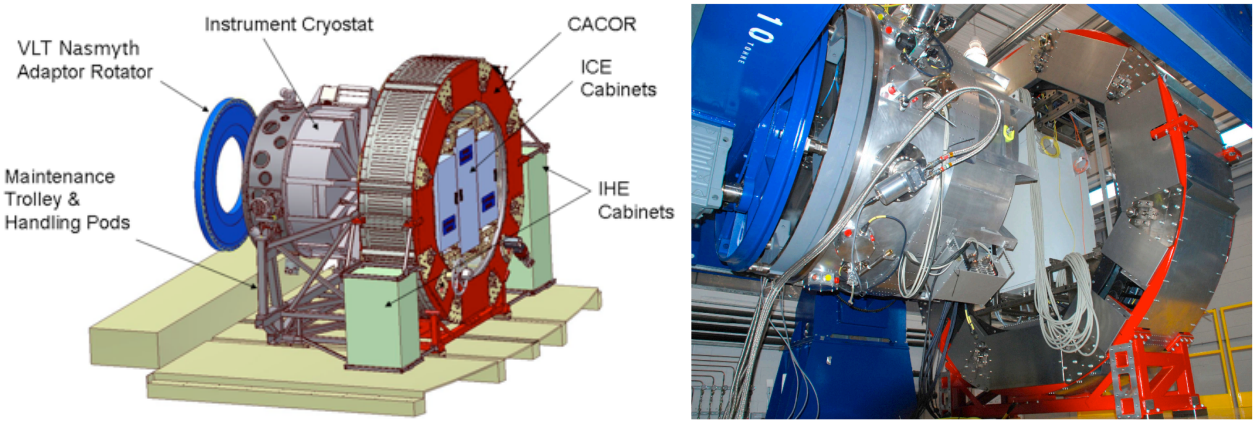

Figure 1: Schematic view of KMOS on the Nasmyth platform (left) and the instrument on the test rig at UK ATC (right)

2.2 Pickoff system

The selection of the pickoff fields is achieved by means of 24 r-θ telescopic pickoff arms, which patrol the instrument focal plane of 7.2 arcmin diameter. Each pickoff unit contains a pickoff mirror and associated relay optics, which are positioned within the telecentric instrument focal plane by means of an articulated arm. The pickoff arms are arranged into two different planes ("top" and "bottom") of twelve arms each, so that adjacent arms cannot interfere with each other. One of the planes is placed above the nominal focal plane and one below. Each layer of twelve pickoff arms can patrol 100% of the field. The two motions (radius and angle) of the pickoff arms are both driven by stepping motors, which are modified for cryogenic operation. Whilst the positioning of the arms is open-loop via step-counting from datum switches, there is a linear variable differential transformer (LVDT) encoder on each arm which is used to check for successful movement. In addition a hardware collision-detection system is also implemented as a third level of protection which can sense if any two arms have come into contact with each other and will stop the movement of the arms within 10μm. All 24 arms can be commanded to move simultaneously and a typical arm movement takes ~120 seconds.

Figure 2: One of the pickoff arms (left) and the full 24 pickoff arm module in the front end of the KMOS cryostat (right)

The tip of each pickoff arm holds a fold mirror to divert the input beam along the arm. A lens is used to collimate the beam and re-image the telescope pupil onto a 4% undersized cold stop. A roof mirror which moves in a direction opposite to the fold mirror maintains the optical path length to the cold stop. A subsequent fold mirror then directs the beam along the arm's rotational axis towards a K-mirror assembly. This element is used to focus the pickoff field onto the intermediate focal plane and also to orient each of the 24 fields correctly onto the IFU image slicers. A set of bandpass order-sorting filters is used to select the appropriate waveband for each observation. As the filters are located in the converging beam produced by the K-mirrors, they are also utilised to correct the chromatic aberrations (focus) introduced by the singlet collimating lens in the arm.

2.3 Integral field units and filters

The integral field units (IFUs) contain a set of fore-optics that collect the output beam from each of the 24 pickoffs and reimage it with appropriate anamorphic magnification on the image slicers. The IFU sub-system has no moving parts and uses gold-coated surfaces diamond-machined from rapidly solidified aluminium (RSA) for optimum performance in the near-infrared and at cryogenic temperatures[6]. The anamorphic magnification is required in order that the spatial sampling pixels ('spaxels') on the sky are square whilst maintaining Nyquist (2-pixel) sampling of the spectral line profile on the detector in the spectral dimension. The slices from groups of 8 IFUs are aligned and reformatted into a single 254mm long slit at the entrance to each of the three spectrometers. The optics in a single IFU therefore comprise: two off-axis aspheric re-imaging mirrors, a third re-imaging mirror defined with a more complex geometry using Zernike polynomials, one monolithic slicing mirror array containing 14 slices with spherical surfaces in different orientations, two monolithic pupil mirror arrays containing 7 facets each with spherical surfaces, and one monolithic slit mirror array containing 14 facets with toroidal surface form. All of the micro-optics in the IFUs are produced by diamond-machining using a combination of diamond-turning and raster fly-cutting techniques. This allows arrays of multi-faceted components to be manufactured with in-built mounting surfaces, all to sub-micron accuracy (Fig. 3). Particular attention

was paid to minimising the micro roughness on the optical surfaces which was in the range 5-10nm rms for most of the components. Detailed metrology measurements[7] were performed on every element to ensure that the stringent tolerances on form error and alignment for the IFUs had been achieved. Fig. 3 shows the completed optical components required for one set of 8 IFUs (384 optical surfaces).

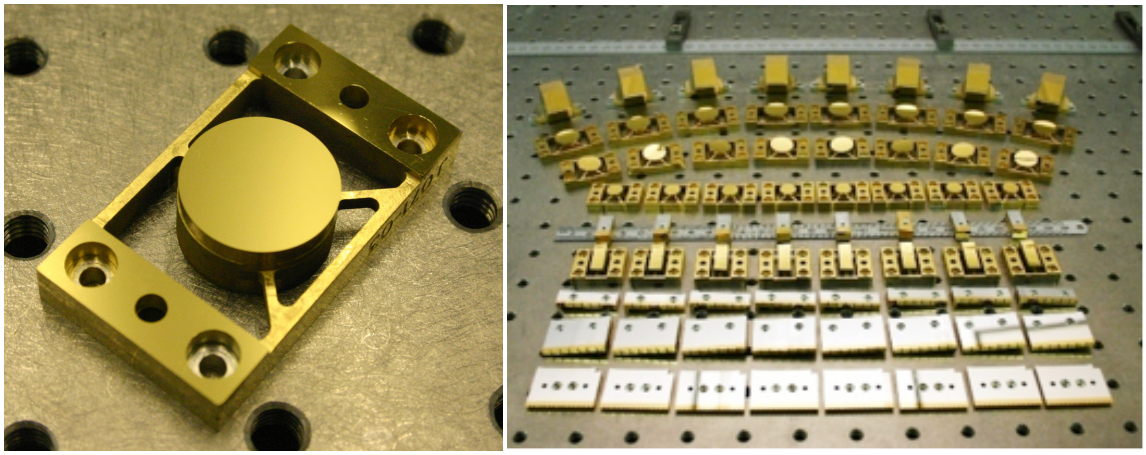

Figure 3: Fore-optics mirror with support (left) and one of three complete sets of IFU mirrors before assembly (right)

2.4 Spectrographs

The spectrograph sub-system[5] is comprised of three identical units, which feed three detectors sub-systems. Each spectrograph uses a single off-axis toroidal mirror to collimate the incoming light, which is then dispersed via a reflection grating and refocused using a 6-element transmitting camera. The five available gratings (IZ, YJ, H, K , H+K) are mounted on a 5-position wheel which allows optimized gratings to be used for the individual bands.

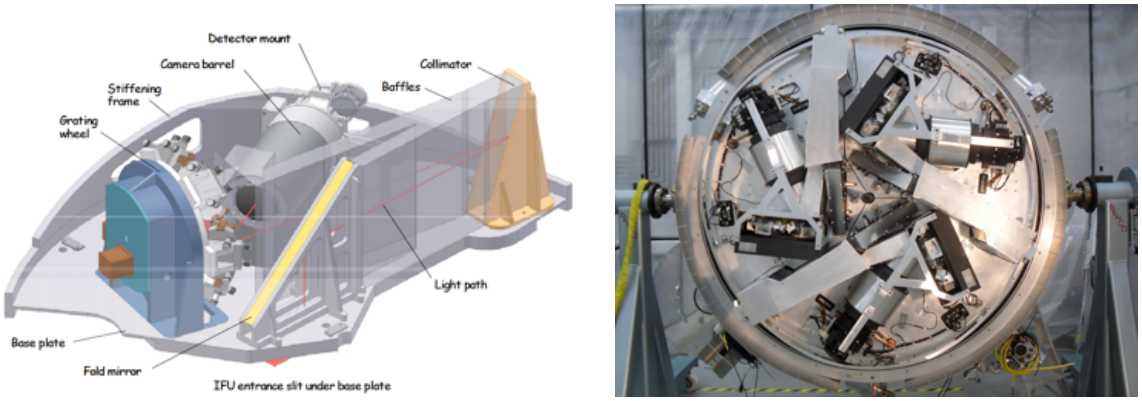

Figure 4: Perspective view of a single KMOS spectrograph module (left) and the 3 spectrograph modules mounted inside the KMOS cryostat (right)

2.5 Detectors

KMOS uses three Teledyne substrate-removed Hawaii 2RG HgCdTe detectors with 2048x2048 18μm pixels (one detector for each spectrograph). The detectors are operated at a temperature of 40K, whilst the rest of the cryostat is at 120K. Typical characteristics are QE>90%, readout noise < $10e^-$ rms for a single double-correlated sample, and dark current < 0.003 e–/sec/pixel). Each detector is adjusted manually for tip-tilt, but is mounted on a remotely operated focus stage. Sample-up-the-ramp (non-destructive) readout is used as standard with Threshold Limited Integration (TLI) to extend the dynamical range for long exposure times. In this mode, if one pixel is illuminated by a bright source and reaches an absolute value above a certain threshold (close to detector saturation), only detector readouts before the threshold is reached are used to compute the slope and the counts written in the FITS image for this pixel are extrapolated to the full exposure time. This is an effective way to remove cosmic rays on these devices[8].

2.6 Calibration unit

Flatfield and wavelength calibration is via an internal calibration unit located inside the cryostat which provides a quasi-uniform light distribution simultaneously to all 24 fields via a 180 mm diameter integrating sphere having 24 output apertures or ports. These ports are divided into sets of 12 (corresponding to the upper and lower level arms) and the light from a specific port is directed toward its corresponding pickoff field via one of 24 calibration mirrors located above the focal plane and just outside the patrol field. All calibration sources, a tungsten lamp for flat fielding and two spectral lamps (argon and neon) for wavelength calibration, are located inside a second external integrating sphere, connected to the internal sphere via a gold-coated light-pipe.

2.7 Infrastructure and electronics

The instrument housekeeping electronics (IHE)[9] are mounted on the Nasmyth platform in two electronics cabinets. The instrument control electronics (ICE)[10] are mounted in a further three electronics cabinets which co-rotate with the instrument. An instrument specific cable co-rotator (CACOR – see Fig. 1) is used to house the ICE cabinets and interface the cables to the instrument (over 1400 wires into the cryostat). This sits on an instrument handling carriage which slides on rails, allowing the instrument to be pulled back to give access to the Nasmyth rotator during maintenance operations. The controller for the cable rotator mechanism is located in a fifth electronics cabinet mounted on the Nasmyth platform to one side of the CACOR.

2.8 Pipeline software

In addition to the above hardware components, a customised data reduction pipeline is being provided for KMOS which will allow the observer to evaluate the data quality after each readout using real-time reconstruction of the data cubes and apply sophisticated algorithms for co-adding of data cubes and subtraction of the sky background. With over 4000 spectra per integration, automatic data processing and reduction methods will be essential to exploit fully the scientific potential of KMOS[11]. The data reduction pipeline will make use of the considerable experience and heritage available from the VLT SINFONI instrument. In addition to instrument control software and housekeeping diagnostics, KMOS will have an optimised pickoff arm allocation tool, known as KARMA, which links directly to the ESO observation preparation software (P2PP). KARMA assigns arms to targets in a prioritised way, whilst ensuring that no invalid arm positions are selected and allows the astronomer to manually reconfigure the list of allocated targets if required[12].

3. OVERALL PERFORMANCE

3.1 Positioning accuracy

The positioning accuracy of the arms is achieved by step-counting from micro switches on each axis. To accurately position the arm in the patrol field requires knowledge of how the arm moves as a function of the number of steps sent to the motors. From a model of the arm motion it was concluded that the error would come primarily from the eccentricity in the lead screws, particularly for the angular motion. The error correction process requires the arm to be moved to a commanded position and the absolute position measured independently. To measure the absolute position requires an accurate measuring device and a FARO laser tracker was chosen with a nominal accuracy of ±10μm (corresponding to 0.02 arcsec in the telescope focal plane). A small retro-reflector was attached to the tip of each arm and the arm was scanned across the full range of its travel. The position of the arm relative to the datum of the laser tracker was then determined and used to define a lookup table of corrections specific to an individual arm. A second look-up table is defined to remove the errors introduced when the arm is mounted into the cryostat. Independent tests of the positioning accuracy in the fully assembled instrument using an X-Y stage with optical encoders indicate that the absolute positioning accuracy of the pickoff mirror is less than ±0.2 arcsec when the instrument is cold.

3.2 Image quality

The specifications for the delivered image quality of KMOS were ≤2 pixels in the wavelength direction and ≤1 pixel in the two orthogonal spatial directions (along and across the image slicers). The spatial image quality across the slice direction is determined only by the optics upstream of the image slicer; along the slice it includes aberrations inside the IFUs and in the spectrographs. Fig. 5 shows one full detector illuminated with an arc calibration lamp (argon and neon) in the H-band. Each detector collects the light from 8 IFUs. As in a traditional long slit spectrograph, the spectrum across

the array is curved by camera distortions, however, this slit curvature is relatively straightforward to correct in software and is done as part of the data reduction pipeline.

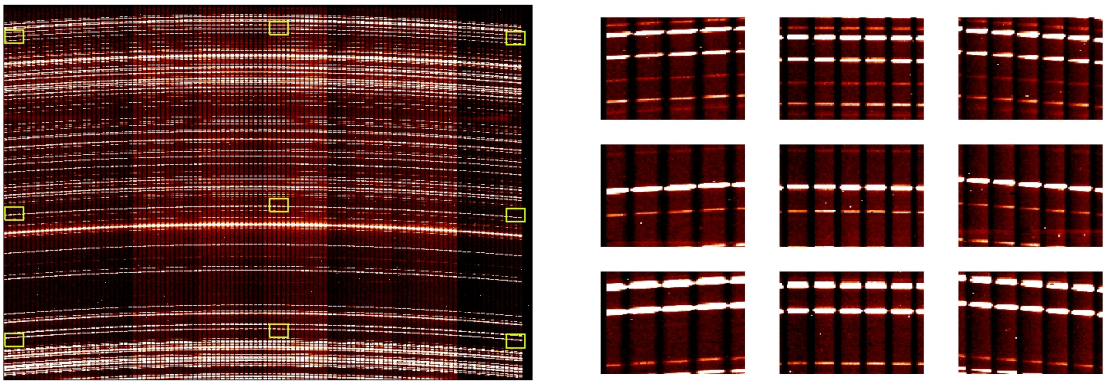

Figure 5: One full detector showing the light from the arc calibration lamp (argon + neon) in the H-band. The yellow squares on the image mark nine positions for which a zoom in is provided in the right panel.

The zoom-in image in the right panel of Fig. 5, shows that the image quality in both spectral and spatial directions is good across the entire array. The measured FWHM of the spectral lines is 2 pixels, providing a good Nyquist sampling of the line profile. In the spatial direction, the image of an unresolved point source, shows a FWHM of < 1 pixel (0.2 arcsec) in the direction across the slices and ~1.3 pixels (0.25 arcsec) in the spatial direction along the slices. In median conditions the additional blurring of 0.3 pixels along the slices corresponds to an increase of only 0.02 arcsec in the apparent FWHM of a point source.

3.3 Spectral bands

KMOS allows observations across five bands, mostly corresponding to the atmospheric windows in the near-infrared. The measured wavelength coverage for each of these bands has been determined from arc line calibration spectra for all three spectrographs and is given in the following table:

Table 2: Spectral coverage for IFUs at the centre of the detector

Band	**Wavelength Coverage (μm)**		
	Spectrograph A	**Spectrograph B**	**Spectrograph C**
IZ	0.678 – 1.092	0.679 – 1.094	0.671 – 1.085
YJ	1.022 – 1.359	1.025 – 1.361	1.015 – 1.352
H	1.452 – 1.866	1.456 – 1.870	1.443 – 1.857
K	1.921 – 2.460	1.922 - 2.461	1.919 – 2.460
H+K	1.474 – 2.471	1.484 – 2.481	1.458 - 2.456

Due to the spectral curvature, not all the IFUs have the same wavelength coverage. The IFUs imaged at the centre of the array have a slightly different wavelength coverage compared to the IFUs at the edge of the array, which are shifted by ~0.01 microns from the above values.

3.4 Spectral resolving power

The spectral resolving power has also been measured from the same arc spectra. The design requirement is defined at the centre of the band and varies with wavelength because of the fixed spectral resolution element in nm. Table 3 gives the resolving powers obtained across all 5 grating settings.

Table 3: Spectral resolving power

Band	Pixel scale nm/pixel	Resolving power Short wavelength	Resolving power Band centre	Resolving power Long wavelength
IZ	0.143	2795	3406	3773
YJ	0.165	3089	3582	4088
H	0.203	3570	4045	4555
K	0.266	3809	4227	4883
H+K	0.489	1514	1985	2538

3.5 Sensitivity

The total efficiency of KMOS in all bands has been measured in the lab using a black body source. The measurements were taken in all bands, but are most reliable for the K-band (Fig. 6). Definitive throughput measurements will be obtained using flux standard stars during commissioning.

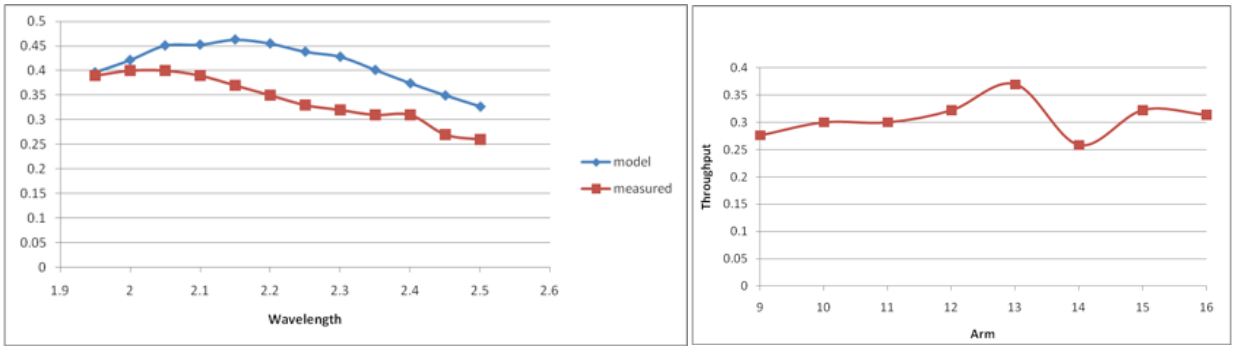

Figure 6: (Left) Throughput measurements across the K-band. The design requirement (>0.30) is defined at the centre of the band (2.2μm) and a drop down to 60% of this at the edges of the passband is allowed in the spec. (Right) Average K-band transmission for all 8 arms in the second spectrograph.

3.6 Ghosts

Because KMOS works in second-order for all of the high dispersion gratings (IZ, YJ, H, K), it is susceptible to first-order Littrow grating ghosts, where the light is reflected back off the detector all the way to the grating and back again. Fig. 7 shows an image in the YJ-band from one of the spectrographs obtained with only one arm in its calibration position fully illuminated with the Argon+Neon lamps. The remaining seven arms are parked in the field outside the calibration position and receive no light. A ghost image is clearly visible on the left of the array; the colour scale has been enhanced to show the ghost, since the level of the ghost is less than 1% of the original signal (for all bands). This ghost image had been predicted by modelling and produces an in-focus image of the science spectrum at lower spectral resolution and with the wavelengths reversed. The ghost also appears on the opposite side of the array with respect to the position of the arm that generates it. The intensity of the ghosts vary slightly from detector to detector, but on average it is: 0.6% in IZ band; 0.4% in YJ; 0.06% in H and 0.2% in K. The ghost covers only a fraction of the observable wavelength, especially in the IZ and YJ bands, because of the lower dispersion. The ghosts produced by bright OH lines are, in the vast majority of cases, well below the level of the intra-OH continuum, except for the very brightest OH lines in the H-band.

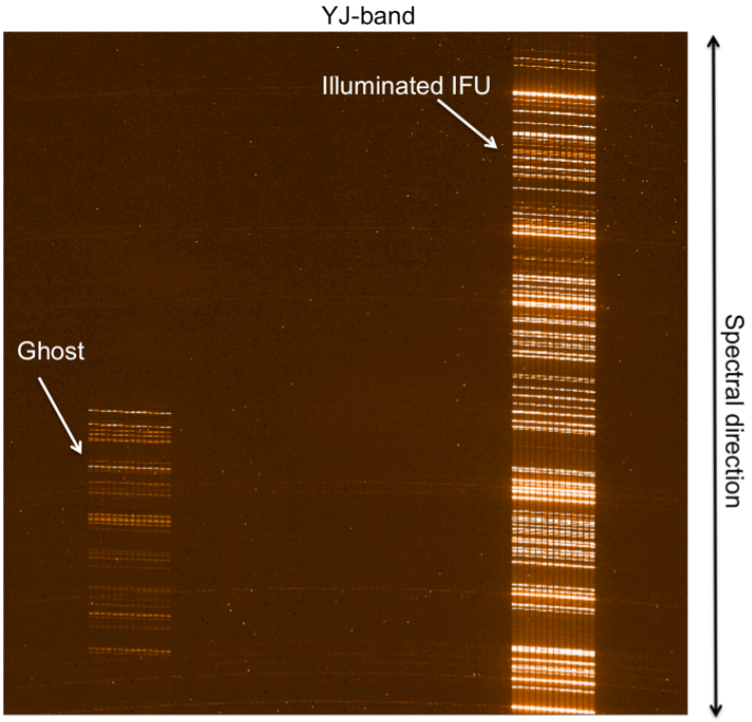

Figure 7: Image in the YJ-band, with one single IFU illuminated with a Argon+Neon calibration lamp (on the right). The ghost is visible on the left side of the array.

3.7 Flexures

Three different types of flexure can affect observations with KMOS: (1) the flexure of the bench; (2) the flexure of the pickoff arms; (3) the flexure of the spectrographs. The first two affect the spatial position of the source on the IFUs, whilst the last one produces a shift mainly in the spectral direction. However, all of them are small and their effect is mostly corrected in software.

The flexure of the bench and pickoff arms due to gravity has a net effect of spatially displacing the targets on the IFUs. However, this shift is always in the opposite direction to the gravity vector and during a complete rotation (360º) the image of the source moves on the field-of view of the IFU describing a well defined ellipse with semi-major axis = 1.5 pixels (Fig. 8). The effect of this flexure is easily compensated during target acquisition and guiding.

Flexure of the spectrograph does not affect spatial image quality, but produces a shift in the spectral direction of +/- 1 pixel in a complete rotation of 360º (Fig. 8). To compensate for this effect, day-time calibrations (flat field and arcs) are carried out at several different rotator positions (every 60º) to ensure that the flat field is correctly registered for all rotator angles. Otherwise there is no effect on the spectral image quality, as the effect during a single observation is much less than the spectral line width. Co-added frames can also be added together using the sky-lines to refine the spectral displacement.

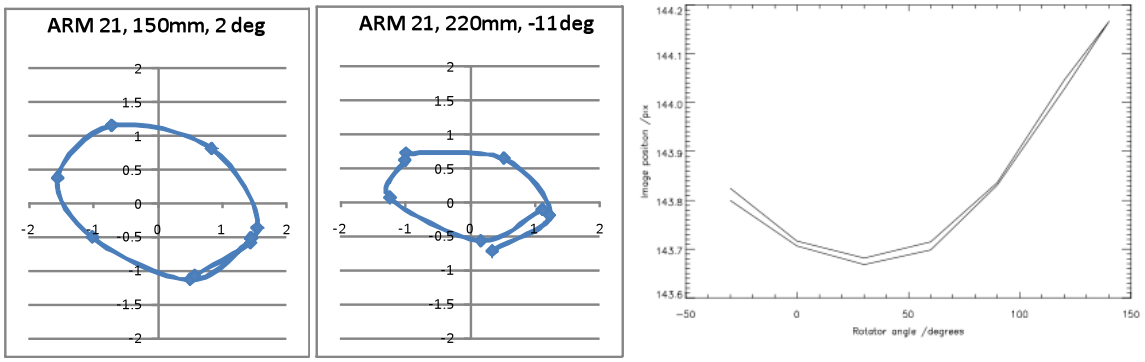

Figure 8: (Left) Spatial flexure for arm 21 at position R=150mm, θ=+2.0 degrees; (Centre) spatial flexure for arm 21 at position R=220mm, θ=-11.0 degrees; (Right) spectral flexure over a 180 degree rotation and back again. In each case the axes refer to pixels at the detector focal plane (18μm).

4. SUMMARY

The KMOS instrument has completed its final integration and test phase and is ready for shipment to the Paranal Observatory for integration with VLT/UT1 (Antu) and on-sky commissioning. Extensive system tests have shown that the instrument is now performing within specification and the first science results from KMOS are expected in Q1 2013.

REFERENCES

[1] Sharples, R., *et al*., "KMOS: an infrared multiple-object integral field spectrograph for the ESO VLT", Proc. SPIE 5492, 1179 (2004).
[2] Sharples, R., *et al*., "Design of the KMOS multi-object integral-field spectrograph", Proc. SPIE 6269, 44 (2006).
[3] Rees, P., *et al*., "KMOS pick-off arm optical alignment, calibration, and testing", Proc. SPIE 7735, 166 (2010).
[4] Dubbeldam, M., *et al*., "Prototyping of diamond machined optics for the KMOS and JWST NIRSpec integral field units", Proc. SPIE 6273, 105 (2006).
[5] Masters, R., *et al*., "KMOS: assembly, integration and testing of three 0.8-2.5 micron spectrographs", Proc. SPIE 7735, 168 (2010).
[6] Dubbeldam, M., *et al*., "An alternative design for a metal image slicing IFU for EAGLE", Proc. SPIE 8450, 56 (2012).
[7] Rolt, S., *et al*., "A review of the KMOS IFU component metrology programme", Proc. SPIE 8450, 23 (2012).
[8] Finger, G., *et al*., "Performance evaluation, readout modes, and calibration techniques of HgCdTe Hawaii-2RG mosaic arrays", Proc. SPIE 7021, 20 (2008).
[9] Bezawada, N., *et al*., "KMOS housekeeping electronics and its functions", Proc. SPIE (2008).
[10] Hess, A., *et al*., "Implementation of the control electronics for KMOS instrument", Proc. SPIE (2010).
[11] Davies, R., *et al*., "KMOS data flow: reconstructing data cubes in one step", Proc. SPIE 7735, 226 (2010).
[12] Wegner, M., *et al*., "Achieving reusability in KMOS instrument software through design patterns", Proc. SPIE 7740, 28 (2010).